De-Novo Design of pre-miR-21 Maturation Inhibitors: Synthesis and Activity Assessment

Iryna Shcheholeva, Daniel Fernández-Remacha, Roger Estrada-Tejedor, Maria Duca, Véronique Michelet

De novo design of pre-miR-21 maturation inhibitors: synthesis and activity assessment

Iryna Shcheholeva[a], Roger Estrada-Tejedor[b], Maria Duca*[a] and Véronique Michelet*[a]

[a] I. Shcheholeva, Prof V. Michelet, Dr M. Duca
Université Côte d'Azur
Institut de Chimie de Nice (ICN), CNRS
Parc Valrose 06100 Nice, France
E-mail: maria.duca@univ-cotedazur.fr, veronique.michelet@univ-cotedazur.fr

[b] Dr R. Estrada-Tejedor
IQS School of Engineering
Universitat Ramon Llull
Via Augusta 390, 08017 Barcelona, Spain

Supporting information for this article is given via a link at the end of the document.

Abstract: Targeting RNA with small molecules is a major challenge of current medicinal chemistry, and the identification and design of original scaffolds able to selectively interact with an RNA target remains difficult. Various approaches have been developed based on classical medicinal chemistry strategies (fragment-based drug design, dynamic combinatorial chemistry, HTS or DNA-encoded libraries) as well as on advanced structural biology and biochemistry methodologies (such as X-ray, cryo-EM, NMR, or SHAPE). Here, we report the de novo design, synthesis, and biological evaluation of RNA ligands using a straightforward and sustainable chemistry combined with molecular docking and biochemical and biophysical studies that allowed us to identify a novel pharmacophore for RNA binding. Specifically, we focused on the targeting of biogenesis of microRNA-21, the re-known oncogene. This led us not only to promising inhibitors but also to a better understanding of the interactions formed between the small molecule compounds and the RNA target paving the way for the rational design of efficient inhibitors with potential anticancer activity.

Introduction

Pharmacological intervention at the RNA level greatly expands the area of accessible biological targets and the discovery of specific ligands of therapeutically relevant RNAs is an emerging area of medicinal chemistry that has already shown its potential.[1] Indeed, a large number of antibiotics, such as aminoglycosides or oxazolidinones, are currently on the market as binders of prokaryotic ribosomal RNA, thus inducing the inhibition of protein synthesis in bacteria.[2] More recently, the FDA approval of Risdiplam as a pre-mRNA splicing modifier for the treatment of spinal muscular atrophy (SMA) highlighted that the field of RNA targeting is just at the beginning of what will probably lead to the discovery of innovative therapies for still incurable diseases.[3] Although RNA targeting has gained a great interest in the medicinal chemistry community over the last decades, the search for compounds able to bind to biologically relevant RNAs and selectively alter their function remains challenging.[4] The most straightforward approach to tackle the problem (i.e. antisense oligonucleotides) proved to be an effective solution, as attested by several approved drugs of this class.[5] However, despite numerous signs of progress made in the field, these modalities still have pharmacodynamic and pharmacokinetic liabilities, mostly caused by nucleases degradation and poor biodistribution. On the other hand, small molecules are often devoid of these problems, yet their selective mutual recognition with nucleic acids is far less intuitive. Oftentimes, ligands found to target secondary RNA structures do not meet the drug-likeness requirements, and once the lead is identified, its potency is difficult to improve.[6]

Among biologically relevant RNAs, microRNAs (miRNAs or miRs) are short non-coding RNAs acting as gene expression regulators upon recognition of mRNAs and inhibition of protein synthesis. Thousands of miRNAs have already been identified in humans, and each of which is responsible for the regulation of the expression of hundreds of proteins, thus having a pivotal role in cellular homeostasis. However, abnormal levels of some miRNAs have been linked to the development of numerous diseases, such as cancers, and several miRNAs have been identified as oncogenic since their overexpression has been directly linked to cancer development and progression.[7] More specifically, miR-21 and its precursor pre-miR-21 (Fig. 1**a**) have been in the spotlight after its consistent overexpression has recently been reported in a study profiling 540 clinical samples from cancer patients.[8] The inhibition of miR-21 function thus holds the promise for both efficient therapy alone,[9a–f] and as an adjuvant to the existing treatments.[10a–e] The search for small molecule inhibitors of miR-21 is mainly based on the targeting of one of its precursors (pri- or pre-miRNA) that bear secondary structures formed by the presence of single-stranded regions (loop and bulges) that together with double-stranded ones induce the formation of specific RNA binding pockets (Fig. 1**a**). During miRNAs biogenesis, Drosha and Dicer ribonuclease cleave the precursors, called pri-miRNAs and pre-miRNAs, respectively, leading to mature miRNAs, but small molecules can bind to the precursors and selectively inhibit miRNA biogenesis. This concept has already been successfully applied in the literature and, in particular, against miR-21 biogenesis.[11a–e] Most of the ligands reported so far to inhibit miR-21, indeed, act by impeding the processing of pre-miR-21 by Dicer (Fig. 1**b**).

Fig. 1. Inhibition of miR-21 biogenesis using synthetic small molecules. a 3D model and schematized structures of pre-miR-21 containing double-stranded and single-stranded regions (single line corresponds to AU pair, double line to GC pair, and single line with a dot to mismatches). If Dicer protein complex cleaves the pre-miRNA-21, the mature miRNA-21 is produced, decreasing the translation of tumour suppressor proteins (example

protein is PTEN PDB:1D5R). Although if a small molecule inhibits this cleavage, no miRNA will be produced resulting in restoring of the tumour suppressor protein levels. **b** Structures of compounds reported in the literature to inhibit miR-21 biogenesis upon binding to pri- or pre-miR-21. **c** A new scaffold presented in this work

During recent years, we developed a multimodal approach for the design of RNA ligands and, in particular, for the discovery of oncogenic miRNAs inhibitors.[11e–d,12a–b] Merging different RNA binding domains in one molecule brought both affinity and selectivity for the target and led us to the identification of compounds capable of inhibiting the biogenesis of oncogenic miRNAs *in vitro* and showing antiproliferative activity in cancer cells with overexpressed targeted miRNA. Although the compounds were not specific for one miRNAs, they were able to selectively target a small set of oncogenic miRNAs and led to a very specific biological effect. Therefore, this multimodal approach thus led to promising results, but the synthetic pathways needed to prepare the compounds were long and tedious, while the compounds themselves bear high molecular weight and unfavorable physicochemical properties for future applications.[11d,12b] Here, we report the *de novo* design of new RNA binders, focusing our effort on developing miR-21 inhibitors bearing good affinity and selectivity but also drug-like properties and synthetic accessibility. To this aim, we have chosen to explore dihydropyrrolopyridine as a privileged and unexplored scaffold to prepare new ligands (Fig. 1**c**). A large series of derivatives were designed and then prepared employing an atom- and step-economical synthetic methodology relying on ruthenium-catalyzed [2+2+2]-cycloaddition thus giving access to the desired scaffold for further functionalization.[13] We brought to light the activities of novel compounds with micromolar affinity for pre-miR-21 and the ability to inhibit miR-21 biogenesis. The detailed study of the potential mechanism of binding using enzymatic footprinting, molecular modeling, and docking as well as STD NMR allowed us to draw convincing structure-activity relationships for a completely new class of RNA ligands.

Results and Discussion

Design and synthesis of a new library of RNA binders. The design of a new RNA-focused library of ligands was driven by modularity and reflection on the data reported so far on the miR-21 inhibitors and binders in general.[11a–b,d,14] Decades after the pioneering report on targeting pre-miRNAs with small molecules[15], the data gathered on the active compounds isn't ample, although some notions of general knowledge in the field are being instilled. Loops and bulges are the primary targets in a search for potential binding sites, being more solvent-accessible and providing more opportunities for the interaction to occur. The logic is supported by the evidence, that the same structures mediate the RNAse recognition of the substrate for subsequent processing, thus abrogating their access by direct ligand binding may result in cleavage inhibition. Some compounds have been reported over the last decade as inhibitors of Dicer processing of the pre-miR-21 *via* direct binding to the pre-miRNA, though, some of them still lack selectivity (Fig. 1**b**).[11a–c,e] *De novo* drug design in academic context without multi-thousand screening libraries at our disposal calls for a careful choice of the starting point. For a purely synthetic approach, referencing known privileged molecular structures can lead to active compounds with a pledge for metabolic stability. Leaning on the broader definition of the privileged scaffold and taking into account the reported RNA binders,[16a–b] we anticipated that the 2-amino-dihydropyrrolopyridine could be a valuable scaffold to construct a new library, able to interact with the target using the two most favorable interactions found in RNA binders, i.e. hydrogen bonds and p-stacking interactions.[17,18] In our continuous research programs towards the preparation of bioactive molecules,[19a–c] and our deep experience in sustainable chemistry, we selected the bicyclic scaffold of dihydropyrrolopyridine, which to the best of our knowledge, has never been envisaged as an RNA binder.

The existing synthetic routes to access the scaffold were not ideal for quick library construction, often involving the preparation of individual nitriles. We thus designed two synthetic strategies allowing for a straightforward and modular synthesis of a large library of compounds involving only 3 steps for the preparation of a common building block (**1a** and **1b** in Scheme 1) followed by functionalization and deprotection steps to obtain the desired compounds (**3a-f** and **4a-4x** in Scheme 1). The key step of our strategies is a ruthenium-catalyzed [2+2+2]-cycloaddition[13b–c,20] constructing the main core from simple precursors, tethered dialkynes **1a-b** and "electron-rich" nitriles **2a-c** or alpha-chloroacetonitrile.

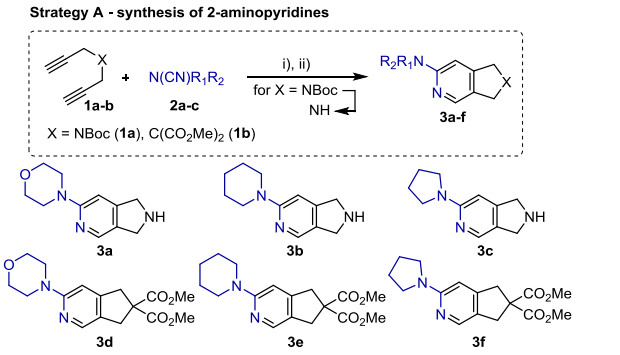

Scheme 1. Strategy A: [a] Reagents and conditions: (i) Cp*Ru(CH_3CN)$_3PF_6$, 2 mol %, DCE, 80 °C, 76-96%; (ii) 5 eq TFA, DCM, 12 h, rt, 82-99%. Strategy B: [a] Reagents and conditions: (i) Cp*Ru(CH_3CN)$_3PF_6$, 2 mol %, DCE, 80 °C, 86%, (ii) 1.3 eq. K_2CO_3, 0.2 KI, 1.3 eq nucleophile, acetonitrile, rt, yield 31-99%, (iii) 5 eq TFA, 2 eq TES, DCM, yield 29-98%; For the modified synthesis of **4l** and **4n** see SI.

This step involves commercially available Cp*Ru(CH_3CN)$_3PF_6$ catalyst and makes synthesis divergent in giving the possibility to employ various dialkyne and nitrile precursors that would deliver a library of differentially decorated core building blocks such as 2-aminopyridines and 2-aminomethylenedihydropyrrolo-[3,2]-pyridines for the final functionalization.

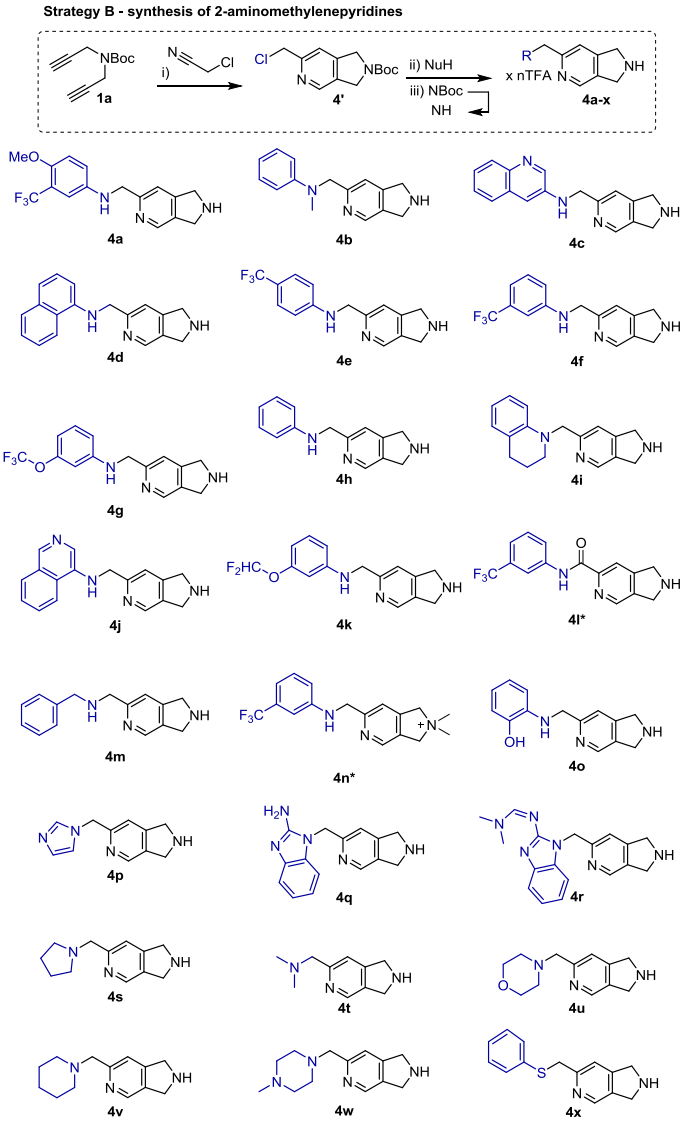

We selected 2 tethered dialkynes, *N*-tert-butoxycarbonyl-protected propargylic alkyne **1a** and the malonate-derived one **1b**, to couple them with a set of cyanamides **2a-c** (Figure S1 in Supporting Information) in the presence of the ruthenium catalyst. The first set of 2-amino-pyridines **3a-f** was isolated in 76-96% yields after the cyclization step and in 82-99% yields after the deprotection step (where applicable) (Scheme 1, Strategy A). In the second, more general strategy, avoiding the preparation of the individual cyanamides, the alpha-chloroacetonitrile **4'** was chosen for the subsequent analogs synthesis (Scheme 1, Strategy B), and was prepared starting from compound **1a** in the presence of Cp*Ru(CH_3CN)$_3PF_6$ catalyst. Pleasingly, we obtained compound **4'** in a very good 86% yield, higher than what was reported in the presence of [Cp*RuCl(cod)] catalyst (56%).[18] This key chlorinated derivative was further substituted using a variety of nucleophiles (compounds **5a-x**, Figure S2 in Supporting Information). The selection of the nucleophiles was based on chemical diversity and drug-likeness considerations and led to the inclusion of anilines with solubility-aiding and fluorine-containing substituents (as in **4a-b,d-i-k-o**), heterocycles, often featuring in RNA-binders (as in **4c,j,p-r**) and of secondary aliphatic amines, such as pyrrolidine, dimethylamine, morpholine, piperidine, and piperazine (as in **4s-w** respectively). Benzylamine (as in **4m**) was further added to probe the optimal length between the aromatic rings and a thiophenol (as in **4x**) replacement was included, as sulfur was recently reported to engage in similar molecular interactions as nitrogen does.[21] The substitution step was optimized by swapping the DMF for acetonitrile as a more sustainable solvent option[22] and conducting the reaction at room temperature in presence of the catalytic amount of KI. The final Boc-deprotection step was conducted with TFA in DCM, with the addition of TES for scavenging the *tert*-butyl cation formed during the reaction.

Lastly, the methylated pyrrolidine and rigid amide in place of benzylic amine group analogs were synthesized. The pyrrolidine ring was methylated (**4n**) to probe the potential importance of this HBD/HBA. The benzylic position derived from the nitrile was swapped for the amide link to test the influence of the rigidification on the scaffold (**4l**). For this purpose, the cyanochloroformate was used in place of chloroacetonitrile in [2+2+2]-cycloaddition with the subsequent hydrolysis of the pyridine ester to the acid, which was coupled with an amine (See SI for synthetic details).

This original and efficient synthetic pathway allowed us to access 30 new and original compounds as unprecedented potential RNA binders. After full characterization of these compounds, we thus moved to the biochemical evaluation of their affinity and activity on pre-miR-21 Dicer processing.

Biochemical evaluation of binding, selectivity and inhibition activity of the synthesized compounds. First, we evaluated the binding of the compounds to the pre-miR-21. The assay we employed uses the 72-mer sequence 5'-labeled with a fluorescent dye and relies on the change in the fluorescence yield upon binding of the ligand to the pre-miR and subsequent modification of the fluorophore environment. We were delighted to see that our *de novo* ligand design resulted in some micromolar binders (Table 1). Among the first set of compounds **3a-f**, only two aliphatic amine analogs have K_D lower than 10 µM, in particular, 7.9 ± 0.1 µM for **3a** and 3.2 ± 0.7 µM for **3b** containing the morpholine and piperidine substitution,

respectively. Compound **3c** has a K_D higher than 10 µM, while compounds **3d-f** did not show any affinity and they were consequently not included in Table 1. Among the second set of compounds **4a-x**, nine (**4a-h,j,k**) have K_D values under 10 µM and compounds **4a,b,c,d,g** bearing the aniline substitution subgroup show K_D lower than 2 µM highlighting the important role of the aniline moiety in binding.

Table 1. Dissociation constant (K_D) values in µM for the synthesized compounds toward pre-miR-21 at 37°C.

ID	K_D (µM)[a]	ID	K_D (µM)[a]
3a	7.9 ± 0.1	**4i**	15.3 ± 1.8
3b	3.2 ± 0.7	**4j**	1.6 ± 0.2
3c	26.9 ± 1.9	**4k**	7.8 ± 2.4
4a	1.9 ± 0.1	**4l**	21.7 ± 1.9
4b	1.6 ± 0.5	**4m**	46.5 ± 0.9
4c	1.9 ± 0.1	**4n**	5.8 ± 0.4
4d	6.4 ± 1.7	**4o**	83 ± 10
4e	2.7 ± 0.4	**4p**	109.7[b]
4f	1.6 ± 0.2	**4q**	49.4 ± 1.5
4g	4.9 ± 1.4	**4r**	28.8 ± 3.2
4h	9.1 ± 1	**4s**	32.5[b]

[a] Binding studies were performed on 5′-FAM-pre-miR-21 in buffer A (20 mm Tris–HCl (pH 7.4), 12 mm NaCl, 2.5 mm MgCl2, and 1 mm DTT). [b] KD values for compounds 4p and 4s have been measured once and the error is estimated at ±10%.

All compounds were then tested for their selectivity in binding pre-miR-21 in presence of a large excess (100 eq.) of competitors such as duplex DNA and tRNA that represent abundant intracellular potential off-targets. Most of the compounds had shown only a small 2 to 3-fold loss in affinity, yet proving the preference for the pre-miR-21 binding over other nucleic acid structures (Table S1). Finally, the best binders, with K_D values below 10 µM, were selected to evaluate their ability to inhibit the Dicer processing of pre-miR-21. For this assay, we employed a double-labeled pre-miR-21 containing a fluorophore (fluorescein) at the 5'-end and a quencher (dabcyl) at the 3'-end. When Dicer cleaves the pre-miR-21, the fluorescence signal will thus increase, while in the presence of an efficient inhibitor, no fluorescence change would be detected. Among the best binders, eight were able to inhibit Dicer cleavage with activities spanning from 43.0 ± 3.0 for **4c** and 57 ± 5 for **4a** to 283 ± 36 µM for **4f** (Fig. 2, Table S2). Compounds **3b**, **4b**, **4g**, **4k**, and **4n** did not show activity.

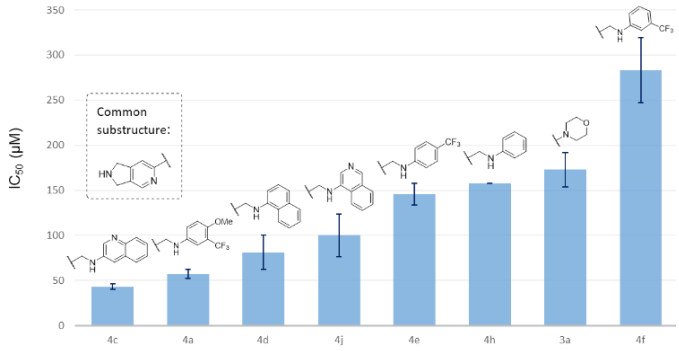

Figure 2. Inhibition activities (IC_{50}, µM) of compounds **4c, 4a, 4d, 4j, 4e, 3b, 4f** and **4b** against pre-miR-21. Assay was performed on 5′-FAM-pre-miR-21-3'-DAB in buffer A (20 mm Tris–HCl (pH 7.4), 12 mm NaCl, 2.5 mm $MgCl_2$, and 1 mm DTT) at 37°C with Human recombinant Dicer.

The aniline substitution proved to be particularly favorable for inhibition since it was present in 7 out of the 8 inhibitors while the morpholine substituent was present in the remaining inhibitor from the aliphatic-substitution group. On the aniline part, the presence of the hydrogen on the aniline is crucial for the activity (no inhibition was observed for the compound **4b**) and CF_3-group in m-/p-position as in compounds **4a, 4f** and **4e** seems optimal for interaction and inhibition (yet analogous m-CHF_2O-/CF_3O-ligands **4g** and **4k** were not active). Alkylation of the pyrrolidine (as in compound **4n**) abrogated the activity, so did the introduction of the linker between aniline nitrogen and benzene ring as in compound **4m**, change of the aniline nitrogen for sulfur as in **4x**, and amide bond rigidification of the scaffold as in compound **4l**.

We, therefore, selected the two best inhibitors **4a** and **4c** as key candidates for the mechanistic studies and further compared them in terms of predicted pharmacokinetics. We found that **4a** had better pharmacokinetic properties, specifically, second best inhibitor had slightly smaller TPSA (49.84 vs 46.18 Å² for **4c** and **4a** respectively), bigger fraction of Csp^3 atoms (0.18 *vs* 0.31)[23a–b] and more hydrogen bond acceptors (3 *vs* 6) (properties calculations were conducted using the swissADME service http://www.swissadme.ch, see SI for details).

Based on the obtained results, we selected compound **4a**, showing the best affinity, inhibition activity, selectivity, and pharmacological properties to study more in detail the mechanism of interaction with pre-miR-21.

Evaluation of binding site and Dicer inhibition using enzymatic footprinting. To perform a detailed mechanism elucidation, we first conducted the Dicer cleavage experiment in the presence of TARBP, an auxiliary protein involved in Dicer processing of the microRNAs and we analyzed the results by denaturing gel electrophoresis. The incubation of pre-miR-21, whose primary and secondary structure are shown in Fig. S4**a**, with compound **4a** and subsequent addition of the TARBP:Dicer complex had shown a concentration-dependent inhibition of pre-miR-21 cleavage located at G28-A29 residues (Fig. S4**b**). To infer more information on the putative binding site, we also conducted footprinting experiments in the presence of RNAse ONE, a ribonuclease catalyzing the hydrolysis of RNA (to cyclic nucleotide monophosphate (NMP) intermediates) at the majority of nucleotides.[24] Having a broader range of visible nucleotides for footprinting allowed us to see a more representative picture of where the binding site is likely located (Fig. S4**c**). The band quantitation revealed dose-dependent inhibition of the cleavage at the nucleotides G28-A29 (abrupt inhibition at the highest concentration was also observed for nucleotides G22-A23, although above the IC_{50} value) suggesting that **4a** is binding selectively at the cleavage site of Dicer thus inhibiting its processing.

Since RNA flexibility doesn't allow drawing direct conclusions from such an experiment as the binding-induced proximal conformational change can be misleading, we decided to apply molecular modeling to confirm these experimental results. Molecular modeling would be useful not only for binding site elucidation but could also guide us in refining the hit molecule and developing a more potent ligand.

Molecular Modeling studies. To probe the binding site hypothesis obtained *via* footprinting, the binding mechanism of **4a** was predicted *in silico* by means of molecular docking against pre-miR-21 structure. Given the inherent flexibility of the RNA structure, the conformation to be used in docking was assessed by Molecular Dynamics (MD) simulations, identifying the most representative structure, in terms of population. Docking on pre-miR-21 structural model showed a significant preference of active ligands over non-active ones in binding to two separate sites (involving the stem and loop regions, near G18 and U43 residues, respectively) that were further investigated *via* molecular dynamics (MD) simulation. MD trajectories analysis revealed significant stability differences between the two poses, the pose on the loop had lower RMSD

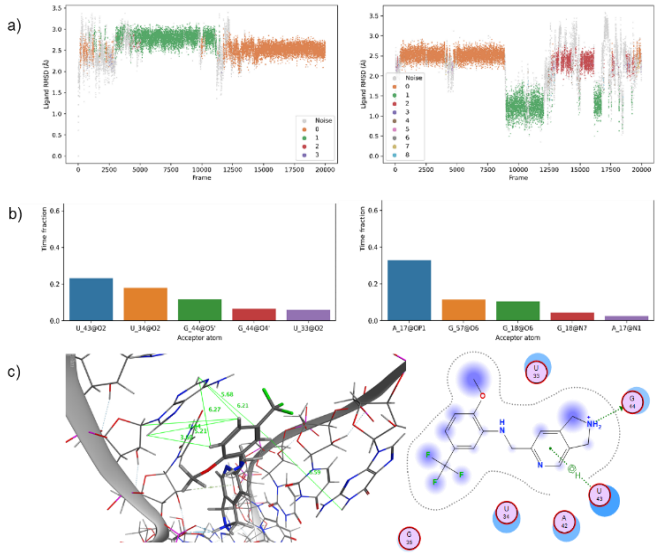

values (30.8 ± 9.3 Å vs 32.4 ± 12.8 Å, elevated values in both cases are expected due to the flexibility of the microRNA, Fig. 4**a**).

Figure 4. Molecular dynamics simulations and docking. **a** Ligand (**4a**) RMSD during simulation trajectory, colored by cluster analysis. Results are shown for the two main interaction sites identified in docking: U43 region (left) and G18 region (right). **b** Relative times vs nucleotides involved in the interaction with **4a** (poses U43 and G18 from the left to the right). C) Molecular representation of the most probable interaction mechanism between **4a** and pre-miR-21 model found: measured distances between ligand hydrogens and receptor (left), mapped interaction legend, size of the purple radii correlates with the physical proximity (right).

Hydrogen bonding analysis also showed higher relative interacting times of the first (loop) pose (77%) compared to the second (stem) (63%), which could also indicate higher stability, as shown in Fig. 4**b** (left and right panels, respectively). Visual inspection of the trajectory obtained from the 1st docking pose revealed that the main binding mode is given through a steady anchoring of the pyrrolidinic nitrogen between ligand and receptor and a parallel conformation to the pre-miR. Cluster analysis of the simulation led to the identification of three main states, with one being predominant over most of the simulation time (Fig. 4**c**) This pose was then used as a reference for comparison with the experimental results obtained in the laboratory.

Epitope mapping via STD-NMR. Finally, we decided to couple the STD NMR with molecular docking and MD simulation to find the concurrent hints on the mode and site of interaction. The low micromolar affinity value is an ideal point to engage this type of NMR experiment, as the complex formation should be sufficiently "loose" and the ligand residence time in a complex should allow liberating some of the bound ligand back into solution within the timescale of the measurement. In conducting the multifrequency measurements, we wanted to adopt a differential STD NMR procedure, largely known for proteins, that can be very useful when juxtaposing the data with docking poses. Moreover, the lower proton density of RNA compared to that of the proteins could help to make the difference more pronounced, as was showcased in the literature.[25] Thus, acquiring the data after irradiation at 4.1, 5.7 and 7.8 ppm, we would observe the saturation transfer from the sugar backbone; non-exchangeable protons at C5 of the uridine and cytosine (pyrimidine bases), C1 of the sugar ring; and C8 guanine and adenine (purine bases), C6 uridine and cytosine, C2 adenine respectively (the data was taken from the available NMR assignment for the pre-miR-21 pre-element) (Fig. 5**a**).[26]

The plotted intensities observed for compound **4a** for each ligand proton (Fig. 5**b**) directly reflect their physical proximity to the biomolecule (different colors refer to different irradiation frequencies). To our delight, the relative acquired STD-NMR signal intensities of the ligand protons correlated well with their physical proximity to pre-miR-21 in the complex after MD simulation. The benzylic protons' analysis was omitted since they overlapped with the water signal. Overall, the pyridine meta-positioned proton (**ε**, Fig. 5**c**) had shown the biggest STD intensities, hence it is closest to the pre-miRNA in the complex. It has also shown more saturation transfer from the aromatic non-exchangeable protons, than from the sugar backbone. This was rather surprising given that most of the dockings showed repeated interaction of the benzylic nitrogen with the sugar backbone, which would place the pyridine protons not too far from it. Vicinal aniline protons followed (**γ-δ**, Fig. 5**c**), on the contrary with higher saturation transferred from the sugar backbone. The ortho-pyridine proton (**ζ**, Fig. 5**c**) has shown slightly lower intensity, with yet bigger importance of the sugar saturation transfer. The isolated aniline proton (**β**, Fig. 5**c**) was closing the aromatic protons rank and the methoxy-group (**α**,

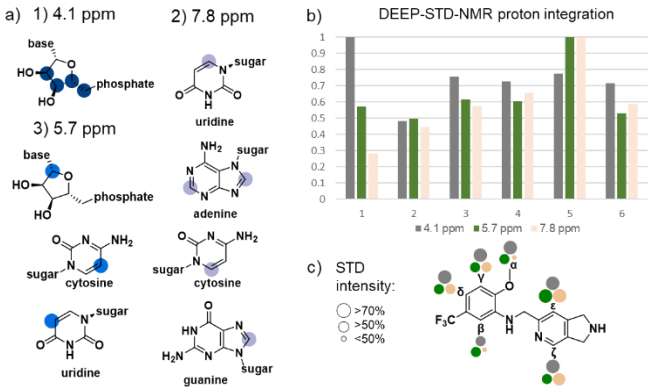

Fig. 5**c**) was preferentially saturated at 5.7 ppm.

Figure 5. DEEP-STD-NMR (Differential-Frequency Saturation Transfer Difference NMR) **a** Differential irradiation frequencies, **b** interaction intensity histogram (y-axis) of different ligand **4a** protons (x-axis), **c** epitope mapping of ligand **4a.** Samples for the STD-NMR study were prepared in buffer C, a phosphate buffer containing 75 μM $Na_2HPO_4{\cdot}7(H_2O)$, 25 μM $KH_2PO_4{\cdot}H_2O$ and

2.5 mM $MgCl_2$ in D_2O, pH 7.4, an additional amount of DMSO-d6 ≤ 10% was used to aid the solubility of the ligand. The ratio of the ligand to pre-miR-21 was 1000:1 with the final ligand concentration 1 mM.

The absence of the rigid pockets on the RNA puts fewer constraints on the solid "black and white" mode of binding, leaving room for discrepancies in the models coming from the different experiments. These results taken together with modeling studies indicate the high involvement of the dihydropyrrole nitrogen of **4a** in the hydrogen-bond interaction with G44 and pyridine ring anchored *via* accepting H-bond from U43. The aniline moiety likely provides a well-positioned hydrophobic consolation to A42 and U43 nucleobases while not intercalating. Close inspection of the pose suggests several sites for further modification of the compounds in view of optimization of the biological activity, namely, ortho-vector on the aniline ring, free ortho-position of the pyridine and dihydropyrrole nitrogen with preservation of its ability to engage in H-bonding.

Conclusion

In conclusion, we have synthesized an RNA-focused library targeted against the production of the oncogenic microRNA-21 and discovered 2-amino-dihydropyrrolo-[3,2]-pyridine and 2-aminomethylene-dihydropyrrolo-[3,2]-pyridine as new and original scaffolds for RNA binding. The synthesis was designed and optimized to deliver the compounds in 5 steps in good yields employing sustainable chemistry. Five compounds bear low micromolar affinities towards pre-miR-21, good selectivity against other nucleic acid structures and promising inhibition activity on the Dicer processing of the pre-miR-21 in the two-digit micromolar range. The mechanism of action was studied in depth with enzymatic footprinting and molecular modeling and allowed us to confirm that trifluoromethylaniline derivative is an efficient binder of the cleavage site of Dicer on the pre-miR-21 sequence. STD NMR allowed us to identify the parts of the most active compound that bind the target showing great accordance with the molecular modeling study. Altogether, the obtained results allowed us to establish unprecedented structure-activity relationships and identify the most promising modifications that could be introduced in the future for ligand optimization that is currently ongoing.

Acknowledgements

This research has received funding from the French government through the UCAJEDI Investments in the Future project with the reference number ANR-15-IDEX-01, Region PACA and BoostUrCareer project European Union's Horizon 2020 research and innovation program under grant agreement no. 847581. M.A. and V.M. also acknowledge Université Côte d'Azur and Centre National de la Recherche Scientifique (CNRS). This study was partly supported by research funding from the Canceropôle PACA, Institut National du Cancer and Région Sud. We are grateful to Dr Marc Gaysinski (Université Côte d'Azur) for the help with STD-NMR and Daniel Fernández Remacha (IQS School of Engineering) for the careful guidance of our MD experiments.

Keywords: drug discovery • inhibitors • RNA • binding mechanism • oncogenes

[1] J. L. Childs-Disney, X. Yang, Q. M. R. Gibaut, Y. Tong, R. T. Batey, M. D. Disney, *Nat. Rev. Drug Discov.* **2022**, *21*, 736–762.

[2] D. N. Wilson, *Nat. Rev. Microbiol.* **2014**, *12*, 35–48.

[3] H. Ratni, M. Ebeling, J. Baird, S. Bendels, J. Bylund, K. S. Chen, N. Denk, Z. Feng, L. Green, M. Guerard, P. Jablonski, B. Jacobsen, O. Khwaja, H. Kletzl, C.-P. Ko, S. Kustermann, A. Marquet, F. Metzger, B. Mueller, N. A. Naryshkin, S. V. Paushkin, E. Pinard, A. Poirier, M. Reutlinger, M. Weetall, A. Zeller, X. Zhao, L. Mueller, *J. Med. Chem.* **2018**, *61*, 6501–6517.

[4] J. P. Falese, A. Donlic, A. E. Hargrove, *Chem. Soc. Rev.* **2021**, *50*, 2224–2243.

[5] S. T. Crooke, B. F. Baker, R. M. Crooke, X. Liang, *Nat. Rev. Drug Discov.* **2021**, *20*, 427–453.

[6] K. D. Warner, C. E. Hajdin, K. M. Weeks, *Nat. Rev. Drug Discov.* **2018**, *17*, 547–558.

[7] M. Winkle, S. M. El-Daly, M. Fabbri, G. A. Calin, *Nat. Rev. Drug Discov.* **2021**, *20*, 629–651.

[8] S. Volinia, G. A. Calin, C.-G. Liu, S. Ambs, A. Cimmino, F. Petrocca, R. Visone, M. Iorio, C. Roldo, M. Ferracin, R. L. Prueitt, N. Yanaihara, G. Lanza, A. Scarpa, A. Vecchione, M. Negrini, C. C. Harris, C. M. Croce, *Proc. Natl. Acad. Sci. U S A* **2006**, *103*, 2257–2261.

[9] a) H. Yin, G. Xiong, S. Guo, C. Xu, R. Xu, P. Guo, D. Shu, *Mol. Ther.* **2019**, *27*, 1252–1261; b) L. X. Yan, Q. N. Wu, Y. Zhang, Y. Y. Li, D. Z. Liao, J. H. Hou, J. Fu, M. S. Zeng, J. P. Yun, Q. L. Wu, Y. X. Zeng, J. Y. Shao, *Breast Cancer Res.* **2011**, *13*, R2; c) M. Y. Shah, A. Ferrajoli, A. K. Sood, G. Lopez-Berestein, G. A. Calin, *EBioMedicine* **2016**, *12*, 34–42; d) S. H. Javanmard, G. Vaseghi, A. Ghasemi, L. Rafiee, G. A. Ferns, H. N. Esfahani, R. Nedaeinia, *Cancer Cell Int.* **2020**, *20*, 38; e) D. Bhere, N. Arghiani, E. R. Lechtich, Y. Yao, S. Alsaab, F. Bei, M. M. Matin, K. Shah, *Sci. Rep.* **2020**, *10*, 1779; f) A. Ghosh, N. Ranjan, L. Jiang, A. H. Ansari, N. Degyatoreva, S. Ahluwalia, D. P. Arya, S. Maiti, *Mol. Ther. Nucleic Acids* **2022**, *27*, 685–698.

[10] a) B. Lahooti, S. Poudel, C. M. Mikelis, G. Mattheolabakis, *Front. Oncol.* **2021**, *11*; b) Y. Li, Y. Chen, J. Li, Z. Zhang, C. Huang, G. Lian, K. Yang, S. Chen, Y. Lin, L. Wang, K. Huang, L. Zeng, *Cancer Sci.* **2017**, *108*, 1493–1503; c) C. Gong, Y. Yao, Y. Wang, B. Liu, W. Wu, J. Chen, F. Su, H. Yao, E. Song, *J. Biol. Chem.* **2011**, *286*, 19127–19137; d) M. Mei, Y. Ren, X. Zhou, X. Yuan, L. Han, G. Wang, Z. Jia, P. Pu, C. Kang, Z. Yao, *Technol. Cancer Res. Treat.* **2010**, *9*, 77–86; e) U. K. Sukumar, R. J. C. Bose, M. Malhotra, H. A. Babikir, R. Afjei, E. Robinson, Y. Zeng, E. Chang, F. Habte, R. Sinclair, S. S. Gambhir, T. F. Massoud, R. Paulmurugan, *Biomaterials* **2019**, *218*, 119342.

[11] a) P. Zhang, X. Liu, D. Abegg, T. Tanaka, Y. Tong, R. I. Benhamou, J. Baisden, G. Crynen, S. M. Meyer, M. D. Cameron, A. K. Chatterjee, A. Adibekian, J. L. Childs-Disney, M. D. Disney, *J. Am. Chem. Soc.* **2021**, *143*, 13044–13055; b) J. S. Matarlo, L. R. H. Krumpe, W. F. Heinz, D. Oh, S. R. Shenoy, C. L. Thomas, E. I. Goncharova, S. J. Lockett, B. R. O'Keefe, *Cell Chem. Biol.* **2019**, *26*, 1133-1142.e4; c) S. P. Velagapudi, M. G. Costales, B. R. Vummidi, Y. Nakai, A. J. Angelbello, T. Tran, H. S. Haniff, Y. Matsumoto, Z. F. Wang, A. K. Chatterjee, J. L. Childs-Disney, M. D. Disney, *Cell Chem. Biol.* **2018**, *25*, 1086-1094.e7; d) C. Becquart, M. Le Roch, S. Azoulay, P. Uriac, A. Di Giorgio, M. Duca, *ACS Omega* **2018**, *3*, 16500–16508; e) C. Maucort, D. D. Vo, S. Aouad, C. Charrat, S. Azoulay, A. Di Giorgio, M. Duca, *ACS Med. Chem. Lett.* **2021**, *12*, 899–906.

[12] a) T. P. A. Tran, S. Poulet, M. Pernak, A. Rayar, S. Azoulay, A. Di Giorgio, M. Duca, *RSC Med. Chem.* **2022**, *13*, 311–319; b) D. D. Vo, T. P. A. Tran, C. Staedel, R. Benhida, F. Darfeuille, A. Di Giorgio, M. Duca, *Chem. Eur. J.* **2016**, *22*, 5350–5362.

[13] a) K. P. C. Vollhardt, *Angew. Chem. Int. Ed. Engl.* **1984,** *23,* 539-556; b) F. Ye, M. Haddad, V. Ratovelomanana-Vidal, V. Michelet, *Org. Lett.* **2017**, *19*, 1104–1107; c) F. Ye, M. Haddad, V. Michelet, V. Ratovelomanana-Vidal, *Org.*

Chem. Front. **2017**, *4*, 1063–1068; d) H. Chowdhury, A. Goswami *Adv. Synth. Catal.* **2017**, 359, 314-322; e) D. Bhatt, N. Patel, H. Chowdhury, P. V. Bharatam, A. Goswami *Adv. Synth. Catal.* **2018**, *360*, 1876-1882.

[14] A. L. Garner, D. A. Lorenz, J. Sandoval, E. E. Gallagher, S. A. Kerk, T. Kaur, A. Menon, *ACS Med. Chem. Lett.* **2019**, *10*, 816–821.

[15] K. Gumireddy, D. D. Young, X. Xiong, J. B. Hogenesch, Q. Huang, A. Deiters, *Angew. Chem. Int. Ed.* **2008**, *47*, 7482–7484.

[16] a) N. F. Rizvi, J. John P. Santa Maria, A. Nahvi, J. Klappenbach, D. J. Klein, P. J. Curran, M. P. Richards, C. Chamberlin, P. Saradjian, J. Burchard, R. Aguilar, J. T. Lee, P. J. Dandliker, G. F. Smith, P. Kutchukian, E. B. Nickbarg, *SLAS Discov.* **2020**, *25*, 384–396; b) B. S. Morgan, J. E. Forte, R. N. Culver, Y. Zhang, A. E. Hargrove, *Angew. Chem. Int. Ed.* **2017**, *56*, 13498–13502.

[17] a) G. Padroni, N. N. Patwardhan, M. Schapira, A. E. Hargrove, *RSC Med. Chem.* **2020**, *11*, 802–813.

[18] N. Fuller, J. Lowe, **2019**, WO2019032528 (A1).

[19] a) A. Carrër, S. Turban, N. Provost, A. Caliez, G. Lamarche, G. Zanirato, M. Beucher, C. Pean, O. Mirguet, F. Perron-Sierra, V. Michelet, *Bioorg. Chem.* **2019**, *92*, 103243-103248; b) V. Michelet, *Chem. Rec.* **2021**, *21*, 3884–3896; c) Y. Tang, I. Benaissa, M. Huynh, L. Vendier, N. Lugan, S. Bastin, P. Belmont, V. César, V. Michelet, *Angew. Chem. Int. Ed. Engl.* **2019**, *58*, 7977–7981.

[20] F. Ye, F. Boukattaya, M. Haddad, V. Ratovelomanana-Vidal, V. Michelet, *New J. Chem.* **2018**, *42*, 3222–3235.

[21] B. R. Beno, K.-S. Yeung, M. D. Bartberger, L. D. Pennington, N. A. Meanwell, *J. Med. Chem.* **2015**, *58*, 4383–4438.

[22] T. Welton, *Proc. Math. Phys. Eng. Sci.* **2015**, *471*, 20150502.

[23] a) F. Lovering, *Med. Chem. Commun.* **2013**, *4*, 515–519; b) K. E. Prosser, R. W. Stokes, S. M. Cohen, *ACS Med. Chem. Lett.* **2020**, *11*, 1292–1298.

[24] V. Shen, D. Schlessinger, in *The Enzymes* (Ed.: P.D. Boyer), Academic Press, New York, 1**982**, pp. 501–515.

[25] S. Di Micco, C. Bassarello, G. Bifulco, R. Riccio, L. Gomez-Paloma, *Angew. Chem.Int. Ed.* **2006**, *45*, 224–228.

[26] S. Chirayil, Q. Wu, C. Amezcua, K. J. Luebke, *PLoS ONE* **2014**, *9*, e108231.

Entry for the Table of Contents

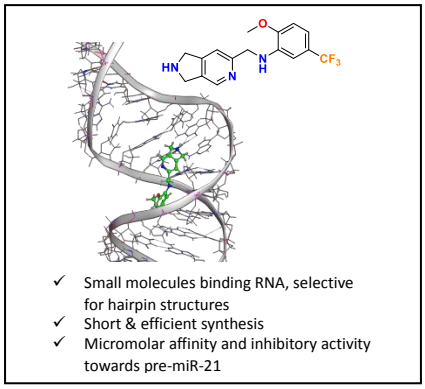

A RNA-focused library targeted against the production of the oncogenic microRNA-21 was designed and synthesized according to a 5 steps sustainable approach. Low micromolar affinities towards pre-miR-2, good selectivity against other nucleic acid structures and promising inhibition activity on the Dicer processing of the pre-miR-21 in the two-digit micromolar range were determined for a trifluoromethyl-functionalized derivative.

Institute and/or researcher Twitter usernames: @NiceChemistry, @MariaDuca_CNRS, @VMichelet06